Article

Plastic Waste Valorization for Fused Deposition Modeling Feedstock: A Case Study on Recycled Polyethylene Terephthalate/High-Density Polyethylene Sustainability

Amira Ragab [1], Rana Elazhary [1], Siegfried Schmauder [2] and Amna Ramzy [1,*]

[1] Faculty of Engineering and Materials Science, German University in Cairo, Cairo 11835, Egypt; amira.abdullah@guc.edu.eg (A.R.); rana.el-azhary@guc.edu.eg (R.E.)

[2] Institute for Materials Testing, Materials Science and Strength of Materials, University of Stuttgart, 70569 Stuttgart, Germany; siegfried.schmauder@imwf.uni-stuttgart.de

* Correspondence: amna.ramzy@guc.edu.eg

Abstract: In this study, material development, characterization, and sustainability assessment are performed on blends from recycled post-consumer commodity plastics for fused deposition modeling (FDM) filament extrusion. A recycled polyethylene terephthalate (rPET) and high-density polyethylene (rHDPE) blend 80:20 ratio is modified using three different methods: compatibilization with Maleic Anhydride, surface functionalization of PET with sodium dodecyl sulphate (SDS), and hybridization by combination of the two methods which is a novel approach. The selected blends were reinforced with chopped glass fibers and characterized. The printability of blends was assessed, and the dimensional accuracy of the prints was calculated. In addition, a cost estimation and comparison between the developed blends and the commercially available FDM filaments was carried out. Finally, life cycle assessment (LCA) was conducted for each prepared blend to facilitate the decision of the optimum blend in relation to mechanical properties and environmental performance and hence correlate the material, economic, and sustainability advantages.

Keywords: sustainability; recycling; compatibilization; functionalization; 3D printing; life cycle assessment

1. Introduction

Additive manufacturing (AM) applications are vastly spreading in the industrial sector and are becoming popular; therefore, the need to integrate sustainability in this method is demanded in order to reduce its environmental impacts [1]. The applications of AM are advancing, including prototyping, mass customization, and creation of any open source design due to its simplicity. The use of AM technologies has increased in various industries such as automotive, food, healthcare, fashion, aerospace, and electronics [1,2]. The use of sustainable raw materials in the AM industry is the main focus of research and development in accomplishing the objective of sustainability with the ultimate goal of achieving a circular economy [3]. The raw materials used in AM applications must be assessed from a life cycle perspective as the decision on material choices will impact the product's over all environmental impact [3].

The largest volume of plastic waste comes from the packaging industry [4], where the three main plastics taking up almost one third of the total were low-density polyethylene (LDPE)/linear low-density polyethylene (LLDPE), polyethylene terephthalate (PET), and high-density polyethylene (HDPE) [5]. The incorporation of the waste commodity plastics as feedstock in AM technology to create a circular economy was reviewed by scientists where all the research focused on either monofilaments, i.e., from only one recycled material or composite filament, i.e., by compounding the recycled plastic with reinforcing fibers/powder [6]. In another study, it was also pointed out that, among the several AM

technologies, fused deposition modeling (FDM) is one of the most plastic-waste-producing methods due to its wide spread among all levels of users and its higher frequency of producing fail prints [7]. Several researches have investigated the use of waste commodity plastics for the production of FDM monofilaments feedstock from waste PET [8], PP [9], and HDPE [10]. PET presents high tensile strength and rigidity as well as good chemical and thermal resistance. These properties enable this polymer to be used as a filament for 3D printing both as virgin or recycled polymer [8,11]. However, PET has its drawbacks, which include low viscosity, moisture absorption, brittleness, and low melt strength [12]. HDPE, whether virgin or recycled, is used to a limited extent in FDM as it possesses ductility, appreciable tensile strength, and high molecular weight which gives it its high viscosity in its molten state [13,14]. The main limitation hindering the use of HDPE as a standard FDM filament is its extreme shrinkage which leads to unpredicted warpage during the printing and hence leads to a high number of fail prints. In addition, HDPE being hydrophobic, with inert surface properties, causes the major problem of not sticking to the printing bed.

On the contrary to mono-materials, polymer blends provide the advantage of combining the properties of more than one material to produce a new material with tailored properties. Several studies have investigated the blending of polymer waste such as PP/PET, PP/Polystyrene (PS) [15], PS/LDPE [16], and PET/HDPE [17]. For the PET/HDPE blends, the results showed that the addition of 10% HDPE to the PET had significantly increased its strain at failure with 10%, while an average drop of the 15 MPa for the stress values were reported. Regarding the thermal properties, no significant change in the melting behaviour of the PET/HDPE blend was reported.

Blends containing PET and HDPE are immiscible due to their incompatible chemical structure, with PET being polar and hydrophilic, while HDPE is non-polar and hydrophobic thus rendering their blend insoluble, so it is necessary to incorporate a compatibilizer in the blend by using block or graft copolymers which are miscible with both components and hence operate at the interface between the two phases by decreasing the interfacial tension and increasing the interfacial adhesion. In addition, some researchers use sodium dodecyl sulphate (SDS) surfactants to treat PET to alter its surface properties in order to increase the chemical bonding between the composite components [18,19].

Life cycle assessment (LCA) is a method frequently used to assess the environmental impact of a product as it takes into consideration a set of impacts for quantitative assessment; therefore, provides an extensive coverage of the product's environmental impact. LCA is used by businesses as it is a powerful decision-making tool. When used properly, it can aid in guaranteeing that a company's decisions are ecologically sensible, whether in the development, manufacture, or use of a product or system. On the financial side, experience has shown that businesses that use LCA can find significant product enhancements and new methods to process optimization [20]. The assessment provided by the LCA methodology takes into consideration all life cycle phases, from raw material extraction up to end of life, including all inputs from the nature and all outputs into the environment [21]. It is becoming increasingly demanded by suppliers to ensure the sustainability of their products. Sustainability is also correlated with the concept of closed-loop recycling where waste materials can be re-introduced to the same process or another process in the form of feedstock and hence circular economy and sustainability are achieved. LCA is used to support the development of more environmentally friendly materials; using LCA when developing material blends of recycled material is important to ensure that the newly developed blend is sustainable in terms of mechanical performance and environmental efficiency since it is becoming increasingly demanded by suppliers. Materials development is extremely useful across sectors and markets for effectively promoting novel material utilization or replacements [22].

In this study, all the aspects of material development are covered by combining material development and life cycle assessment (LCA), and we ensure that the applied LCA is precise since all the experimental procedure, material used, and data are available. This limits the number of assumptions, which is the main issue when conducting an

LCA. This enables one to produce new material using material waste, and then apply life cycle assessment to ensure the sustainability and environmental performance of the newly developed material; hence, this contributes to a reliable, fully examined product.

The aim of this research is to present a novel approach in developing new materials for 3D printing applications by assessing both material and sustainability performance. The newly developed PET/HDPE immiscible blends are of ratio 80:20 were blended using three main approaches: compatibilization, surface functionalization, and hybridization, which is a novel approach by combination of both methods. Glass fiber reinforcement is incorporated with the best performing blends and the overall material and sustainability performance is determined by a series of characterization tests, as well as applying life cycle assessment (LCA) on each blend to assess its environmental impact. This study also provides an investigation of the printability of the developed blends, so that they can be used as an alternative, more sustainable feedstock in AM applications. The study is divided into two tracks the material development track and the life cycle assessment track.

2. Materials and Methods

2.1. Material Development

2.1.1. Materials

Recycled food-grade PET pellets QPET 80 were provided by BariQ for techno and advanced industries, Egypt. Recycled HDPE pellets were obtained from Fostat Trading Company, Egypt. Maleic Anhydride (MA) powder was obtained from Morgan Chemicals, Egypt. The reinforcements added to the blends were glass fibers. The glass fibers (E-glass, diameter: 11–13 µm, length: 4.5 mm) were kindly provided by Hebei Yuniu Fiberglass Manufacturing Co., Ltd., Xingtai City, Hebei Province-China. Sodium dodecyl sulphate (SDS) and benzoyl peroxide (BPO) were purchased from El Mekawy for Import and Trade of Scientific Instruments and Laboratory Products, Cairo-Egypt. Primary antioxidant Irganox 1010 (pentaerythritol tetrakis [3-[3,5-di-tert-butyl-4-hydroxyphenyl] propionate) and secondary antioxidant Irgafos 168 (Tris [2,4-di-tert.-butylphenyl] phosphite) were generously supplied by Ingenia Polymers Corporation, South East Calgary, Alberta-Canada.

2.1.2. Blends Preparation

Recycled control blend (R–Control) was prepared, where 80 wt.% recycled PET (rPET) pellets were hand mixed with 20 wt.% recycled HDPE (rHDPE) pellets. This specific blend composition was chosen based on the previous literature, where several ratios of both polymers were blended using an internal mixer, and it was shown that an 80:20 ratio presented the lowest screw torque and a low specific mechanical energy input which is better in terms of processability [23]. The use of pellets enables the easy implementation of the blend preparation. The control blend was prepared without any additives for comparison to evaluate the effect of compatibilization and surface functionalization on the overall blend properties.

Compatibilization Track

HDPE-g-MA copolymer was added as 5 wt.% of the total weight of the polymers in the blend and the amount of copolymer added to the blend was based on previous studies [24,25]. The HDPE-g-MA was formulated using a technique analogous to that presented in this study [26]. A total amount of 0.4% of BPO and 0.2% of MA powder were added to acetone solution and stirred for 30 min at ambient temperature until all the powder particles have disappeared and dissolved. Then, the RHDPE pellets were added to the solution then left until all acetone has evaporated (blend name: GMA).

Surface Functionalization Track

Functionalization of PET with SDS. PET pellets were added to 1% solution of SDS. Then, they were stirred for 1 h in the solution, then dried in an oven at 100 °C for 1 h. Afterwards, the PET was dried again for 6 h at 100 °C in an oven to remove any retaining moisture (blend name: SDS).

Hybridization Track

Both maleation and surface functionalization methods were employed where the HDPE-g-MA and SDS were blended keeping the same ratio of 80:20 SDS:HDPE-g-MA.

Reinforced Blends

Two reinforced blends were prepared, where chopped strands of glass fiber reinforcement were added. The glass fibers (GFs) were added as 10 wt.% with respect to the total weight of polymers in the blend, where the polymer matrix represents 90% and the glass fibers represent 10% (blend names: GMA-GF, SDS–GF).

The primary antioxidant Irganox 1010 and secondary antioxidant Irgafos 168 were added as 0.06 wt.% and 0.12 wt.%, respectively, with respect to the total weight of the polymers in all blends except R–Control blend hinder further degradation during processing and service life.

2.1.3. Characterization

Thermal Characterization

Differential Scanning Calorimetry (DSC)

Calorimetric characterization was performed according to ASTM D3418 on TA Instruments DSC Q2000 using a heat/cool/heat mechanism under nitrogen gas atmosphere. The first heating run started from 25 °C up to 300 °C with a rate of 10 °C/min to remove previous thermal stresses in the samples, then cooled from 300 °C to 25 °C with the same rate, followed by a second heating run [27]. Reference pan was 20 mg in weight, and average sample weight was around 17 mg. The percentage crystallinity [28] was calculated using Equation (1) below:

$$\%X_c = \frac{\Delta H_m}{\varphi \times \Delta H_m{}^0} \times 100 \ [\%] \tag{1}$$

where ΔH_m is the melting enthalpy of the polymer, φ is the weight fraction of the polymer in the blend, and $\Delta H_m{}^0$ is the theoretical melting enthalpy of 100% crystalline polymer.

Dynamic Mechanical Analysis (DMA)

DMA test was performed to determine the glass transition temperature (T_g) of PET in the blends, the samples were tested using TA Instruments DMA Q800. The testing mode was multi-frequency strain using film tension clamps, with a dynamic deformation amplitude of 1 μm and heating rate at 3 °C/min starting from 25 °C to 200 °C. The frequency was set to 1 Hz. Average sample dimensions were 9.8 × 10.8 × 4.0 mm. One sample was tested for each blend.

Morphological Examination

SEM images were taken using FEI Quanta FEG 250, the fractured impact specimens were photographed using accelerating voltage of 20 kV, spot size 3.5 nm, and circular backscatter detector (CBS). It should be noted that the samples were not gold-sputtered before photographing, so some images are slightly dark due to the charging of the surface from the electrons.

Mechanical Characterization

Tensile and impact samples were injection molded using Fu Chun Shin FT-60 injection molding machine with the following parameters: nozzle temperatures 240–260 °C, screw speed 168 rpm, injection pressure 103 bar, holding pressure 44 bar, and clamping force is 60 tons. Tensile samples were of type I according to ASTM D638, while impact specimens' dimensions were according to ISO 180 [29].

Tensile Test

Specimens were conditioned at room temperature for 24 h before testing. Samples were mechanically characterized according to ASTM D638 using Zwick/Roell Z100 under a strain rate of 5 mm/min. An average of seven samples were tested, and the farthest two

outliers were discarded. The percentage elongation was taken directly from the machine extensometer. The overall length of the specimens was 19 cm. The cross-section dimensions of the gauge length section were 10.5×3.5 mm.

Impact Test

The Charpy impact test was performed according to ISO 180, using Beijing Jinshengxin digital impact tester with hammer energy of 4 joules. The free-fall angle and impact angle were measured by the machine, and then the energy absorbed and impact strength were calculated. Five unnotched samples were tested for each blend and their average was calculated. The sample dimensions were $70 \times 10.5 \times 3.5$ mm.

2.1.4. Filament Extrusion and Assessment

Filament of all blends were extruded on Filabot EX6 Filament Extruder attached to an air cooling path and a filament winding unit. Screw temperature zones ranged at 250–270 °C and 230–240 °C for the nozzle temperature. The selected screw temperatures were chosen based on the PET melting peak obtained from the DSC while considering thermal degradation. The nozzle temperatures were selected to be lower to cool the blend upon exiting the nozzle, for sufficient viscosity to be held and suspended over the air path to be fed and wound onto the spool.

3D Printing and Printability Assessment

The 3D models were drawn using Solidworks software (https://www.solidworks.com/), and the g-code of the model was generated using Ultimaker Cura software (https://ultimaker.com/software/ultimaker-cura/). The filaments were 3D printed using Prusa i3 MK3S+ 3D printer with nozzle temperature 275 °C except the GMA-GF blend which had a nozzle temperature of 285 °C. The printing speed was 40 mm/s, the layer height was 0.4 mm with a print bed temperature of 60 °C, and the nozzle diameter was 0.8 mm with the entire model made of shells. The path width was 0.96 mm to create an overlap between the printed tracks. The printed parts were composed of nine layers from the base upwards. The samples were printed lying flat on the printing bed, so that the loading direction would be parallel to the printed tracks (raster angle = 0°). The dimensions of the 3D printed samples were $70 \times 10.5 \times 3.5$ mm. The fracture surfaces of the samples were photographed using Zeiss Stemi 2000-CS stereo microscope connected to a computer which is equipped with Zeiss Zen microscopy software Blue edition. The average dimensions of the 3D printed parts were also measured using a micrometer to be compared to the initial model dimensions drawn on the computer for dimensional accuracy evaluation.

Cost Comparison of Materials

To evaluate the amount of savings when using recycled materials, the prices of the raw materials used were compared with the prices of currently available spools of the same virgin material. The unit prices of each of the raw materials used in the blend were obtained from the suppliers in Egypt or from Sigma Aldrich website.

2.2. Life Cycle Assessment (LCA)

Life cycle assessment (LCA) was deployed in this study to assess the environmental impacts of 3D printed filaments composed of rPET/rHDPE blends. The guidelines followed to conduct this LCA were ISO 14040 and ISO 14044 [30,31]. The software tool Umberto LCA® (https://www.ifu.com/umberto/lca-software/) was used to model the phases of the life cycle and analyze and calculate the impacts derived in each phase. The methodology was carried out in four stages: goal and scope, life cycle inventory (LCI), life cycle impact assessment (LCIA), and interpretation of the results.

2.2.1. Goal and Scope Definition

The purpose of this LCA is to assess newly developed blends composed mainly of rPET/rHDPE and to provide a complete and reliable environmental performance. The

assessment is expected to identify the environmental impact of the blends in comparison to using virgin material for the 3D printed filaments.

2.2.2. Functional Unit and System Boundary

The functional unit of this assessment was unified to 1 kg for each blend. The system boundary applied was cradle to gate as shown in Figure 1, including the raw material phase which includes all the raw materials used for the blends with all upstream activities included for the raw materials, disregarding the transportation of the raw materials followed by the manufacturing phase which quantifies the material flows and energy flows for each process used to obtain the 3D printing filaments for fused deposition modeling techniques (FDMs).
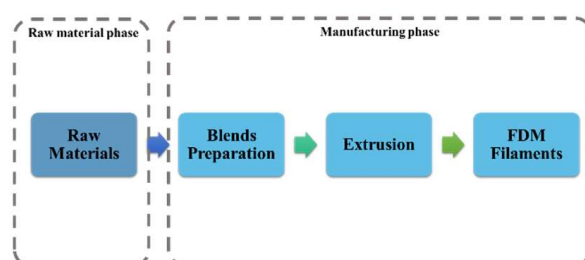

Figure 1. System Boundary.

### 2.2.3. Life Cycle Inventory (LCI)

The essential data for each stage of the LCA have been obtained from the experimental work. Table 1 presents the inventory for each blend, where all the material and energy required to obtain the blend is demonstrated. The life cycle inventory database "Ecoinvent v3" was used for the raw material data for the raw material extraction phase in the LCA; however, Irganox was not available in the Ecoinvent database or the literature, therefore, it was cut-off from the life cycle impact assessment (LCIA) due to its negligible quantity (0.06%). The data for the manufacturing phase were obtained from the experimental procedure as the electricity consumption was calculated based on the extruder's energy consumption and the oven used for drying adding up to approximately 6.2 kWh/Kg.

Table 1. Inventory.

Blend	Blend Composition/Raw Material Inputs								
	rPET (kg)	rHDPE (kg)	Irganox (kg)	Irgafos (kg)	MA (kg)	SDS (kg)	BPO (kg)	GF (kg)	Distilled Water (kg)
R–Control	0.8	0.2	-	-	-	-	-	-	-
GMA	0.8	0.15	0.0006	0.0012	0.025	-	0.025	-	-
SDS	0.8	0.2	0.0006	0.0012	-	0.025	-	-	2.5
GMA-SDS	0.8	0.15	0.0006	0.0012	0.01	0.025	-	-	2.5
GMA-GF	0.8	0.15	0.0006	0.0012	0.025	-	0.025	0.1	-
SDS–GF	0.8	0.2	0.0006	0.0012	-	0.025	-	0.1	2.5

2.2.4. Life Cycle Impact Assessment (LCIA)

The impact assessment provides the quantification of environmental impacts of a product. Umberto LCA® has been used to create a material and energy flow model [32] shown in Figure 2 that includes all inputs, outputs, and processes in each phase of the life cycle being assessed in this study: Phase 1 included all upstream activities for the raw material extraction and Phase 2 included the manufacturing procedure with all inputs to produce the 3D printing filaments.
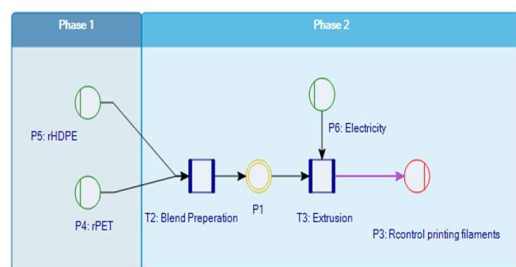
Figure 2. LCA Phases.

ReCiPe Midpoint assessment was used in this study to assess the environmental impacts; the midpoint evaluation considers the effect earlier along the chain of events where it focuses on singular distinct environmental issues. The selected impact categories were selected to show the environmental performance of the filaments: global warming potential, fossil fuel potential, freshwater eco-toxicity potential, human toxicity potential, ozone depletion potential, water consumption potential, terrestrial acidification potential, and particulate matter formation potential.

The LCIA data were obtained either from Ecoinvent database or from the literature. The rPET LCIA was retrieved from our own previous research work [28,33,34] where LCA was conducted to assesses the environmental impact of recycling postconsumer plastic bottles to obtain rPET granulates.

3. Results

3.1. Material Development

3.1.1. Thermal Characterization

DSC

Thermal characteristics obtained for the HDPE and PET polymer components in the blend are presented in Table 2. Here, the change in melting temperature before and after compatibilization was observed as it indicates the compatibility status of the blend components. It was noticed that the melting temperature (T_m) of both HDPE and PET are almost unaffected in all blends, which is expected for polymer blends that are immiscible [35]. The difference in melting temperatures between the blend components is almost unaltered, which could be due to the small wt.% of compatibilizer, as in the study by Taghavi et al. [25] where the difference was notably lower with compatibilizer content of 15 wt.% HDPE-g-MA.

The percentage crystallinity ($\%X_c$) of HDPE in the recycled control blend was 64.8% and decreased significantly in all the blends. The decline in $\%X_c$ in the SDS blend was about 37% with respect to the R–control blend. The GMA blend had a $\%X_c$ lower than the R–Control by almost 62%. The largest decrease was seen in the GMA–GF blend, where the crystallinity dropped by around 66%. This decrease is also seen in a previous study [35], where it was attributed to the interaction of the compatibilizers with the HDPE, which hinders the ability of the chains to orient and form crystals. Furthermore, the lower enthalpy of crystallization (ΔH_c) also confirms that the amount of crystallization of HDPE is lower [36]. As for the $\%X_c$ of PET, it was initially low in the R–control blend, with a value of 18%, and it increased in all the blends. As PET is the major blend component, the presence of HDPE along with the compatibilizer in the matrix act as nucleating agents and hence raise the $\%X_c$ of PET [35].

The largest increase in $\%X_c$ of PET was confirmed in the SDS blend by approximately 36%, this could be attributed to the SDS functionalization which facilitates crystallization by creating nucleation sites [37]. Furthermore, the degradation that occurred to the polymer resulting in chain scissions and shorter chains could be the reason behind the increase in crystallinity. The decrease in crystallization temperature (T_c) in all the blends except the SDS blend could be linked to the degradation of PET [36]. The GMA blend had a T_c

of 198.80 °C, which is 4 °C lower than the R–control blend; this can be explained by the interaction of PET with the grafted compatibilizer (HDPE-g-MA) at the interface between the two polymers, thereby reducing the mobility of the PET chains and hence lowering its crystallization temperature [38], which denotes better compatibility. The T_g of PET of the blends was virtually unaltered in the blends or showed very small differences. The T_g of PET will be discussed as well in the DMA section.

Table 2. Thermal characteristics obtained from DSC curves. Enthalpies of fusion ΔH_m^0 of 100% crystalline HDPE and PET were taken as 293 J/g and 119.8 J/g [39], respectively.

	HDPE					PET					
Blend	T_m (°C)	ΔH_m (J/g)	T_c (°C)	ΔH_c (J/g)	$\%X_c$	T_m (°C)	ΔH_m (J/g)	T_c (°C)	ΔH_c (J/g)	$\%X_c$	T_g (°C)
R–control	132.24	37.96	117.97	50.22	64.8	251.46	17.21	203.15	24.64	18.0	79.45
SDS	132.08	23.87	118.35	25.22	40.7	251.03	27.09	212.35	38.81	28.3	77.96
GMA	133.82	14.47	117.27	15.05	24.7	252.47	21.98	198.8	26.26	22.9	81.58
GMA—SDS	132.8	15.49	117.42	14.28	26.4	251.58	26.45	200.37	31.54	27.6	78.26
GMA–GF	132.49	12.84	118.34	13.16	21.9	251.08	22.97	194.14	28.48	24.0	79.64
SDS–GF	132.78	21.04	118.1	20.92	35.9	251.17	21.94	198.54	25.62	22.9	81.51

DMA

The storage modulus (G′) in Figure 3 represents the elastic component of the viscoelastic material, or the ability of the material to store energy. All the curves decrease with a small slope, which indicates softening of the polymer upon rising temperature [40] or in other words, the chain mobility of the polymer increasing. A steep slope around 80–90 °C denotes the T_g of PET where the chain mobility of the chains is restricted, which agrees with the literature values [41]. It is obvious that the lowest starting G′ value belongs to the R–control blend, which is attributed to the immiscibility between the two polymers [42], where a less elastic or brittle blend is formed due to phase discontinuity. This phase discontinuity is due to large interfacial tension between the two phases and, hence, a decreased contact area. Both SDS and GMA blends show a higher G′ which means the blends are more elastic [43] and more compatible [40], with GMA being more elastic than the SDS blend.
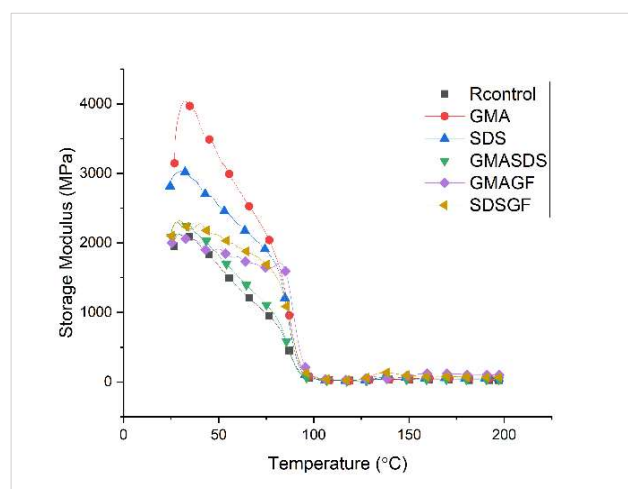
Figure 3. Storage moduli curves of blends.

The GMA–SDS blend shows a low G′ which indicates the lack of miscibility enhancement provided by combining the compatibilization and functionalization techniques. Both GMA–GF and SDS–GF blends show a lower G′, indicating that these blends are stiff

due to the presence of the glass fibers, with GMA–GF having lower G' than the SDS–GF, which leads to conclude that the GMA–GF may exhibit higher ductility in comparison to the SDS–GF, due to better fiber-matrix adhesion provided by the compatibilizer. The slight increase in G' around 125 °C is due to cold crystallization which is a standard PET characteristic [44].

The T_g values present in Table 3 are estimated from the smoothed curves of the Tan Delta (tanδ) component (seen below in Figure 4). The tanδ is the ratio of the G'' to G', which also represents the damping of the material. The peak of the tanδ curve can sometimes be used to give an indication of the T_g despite giving higher temperature values than the DSC. Some blends had faint peaks of loss modulus (G'') curve so the T_g from G'' peak was not located. It is mentioned that the G'' peak expands and locating the T_g will be challenging when the $\%X_c$ increases [45].

Table 3. T_g values from Tan Delta curves.

	R–Control	**GMA**	**SDS**	**GMA–SDS**	**GMA–GF**	**SDS–GF**
T_g from tanδ peak/°C	97.27	95.26	93.94	93.76	96.25	96.78
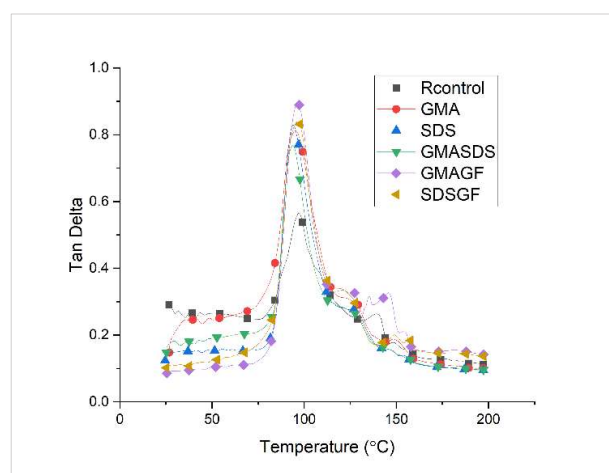


Figure 4. Tan Delta curves of blends.

Henceforth, for simplicity, tanδ peak temperature values were compared as they are the most sensitive factor to morphology. The R–Control shows the highest T_g because of the incompatibility between the blend polymers. The remaining blends show lower T_g, implying that an interaction has occurred between the two polymers due to the presence of the HDPE-g-MA compatibilizer or the PET functionalized with SDS or both. The lowering of the T_g implies that it is approaching the T_g of the other polymer component [15], HDPE, meaning that the compatibilization and functionalization techniques work on enhancing the miscibility between the two polymers. This effect is suppressed in the glass fiber reinforced blends, possibly because the presence of reinforcement restricts the mobility of the polymer chains, hence delaying the glassy to rubbery transition of the PET.

3.1.2. Morphology Examination

SEM images of all the blends are presented in Figure 5. The R–Control blend shows a droplet morphology, where the bright matrix phase is the PET and the dark sphere-shaped dispersed phase is the HDPE. The clear boundaries that separate the HDPE from the PET are an indication of incompatibility [43]. Furthermore, the large size of dispersed particles in the matrix is also a sign of an inhomogeneous blend, and can act as crack initiators yielding low percentage elongation (%EL), hence a brittle blend. Variation in the HDPE particle size has also been reported in an earlier study [46]. The largest HDPE droplet size is 110 μm, obtained from ImageJ software (https://imagej.nih.gov/ij/download.html). The

average was not calculated as the quality of the images did not allow for it. Furthermore, a smooth surface and bright voids can be seen indicating the easy separation of the minor phase from the major phase due to a lack of interfacial adhesion between the PET and HDPE [38,47].
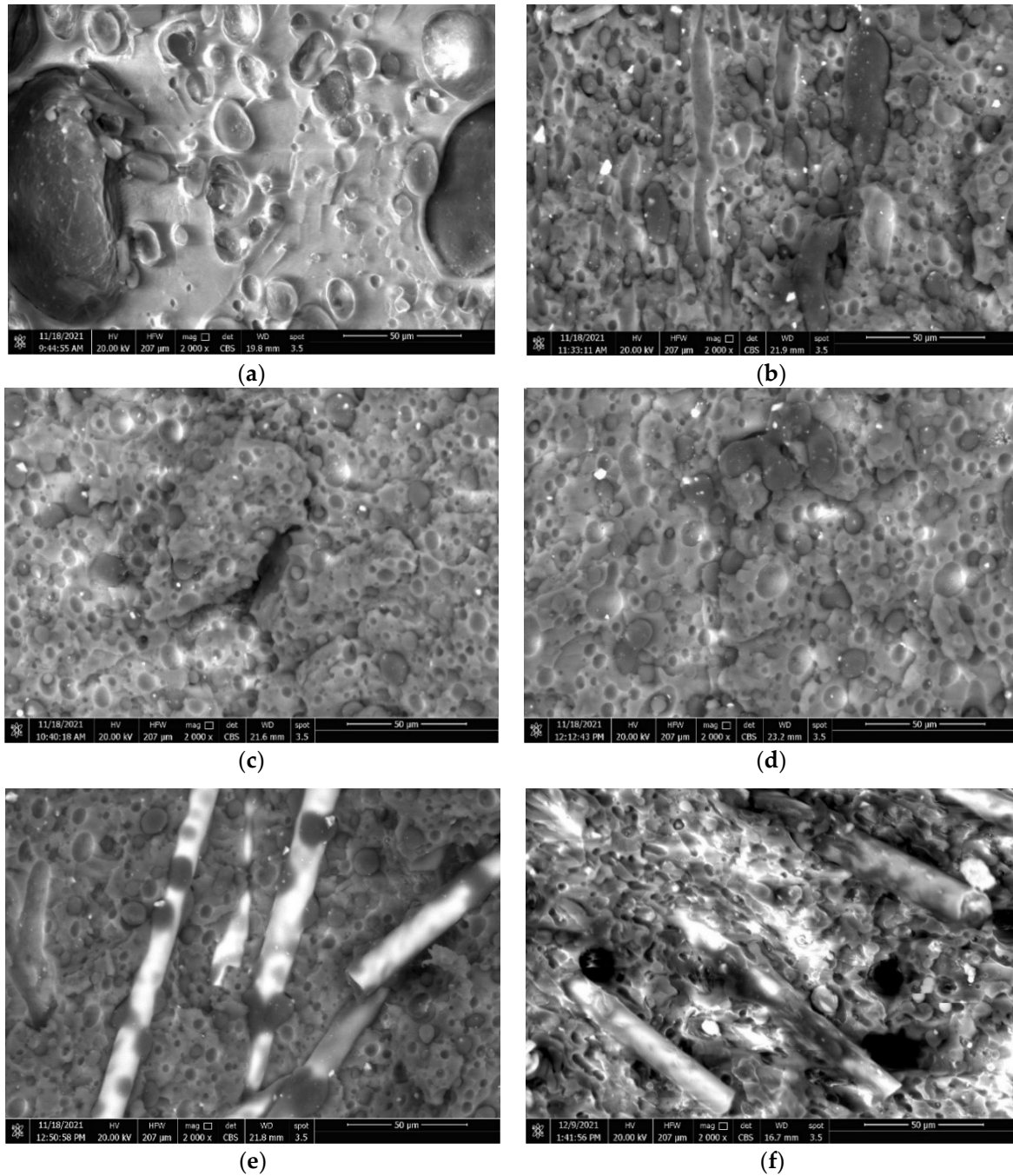
Figure 5. SEM images of the blends at 2000× magnification. (**a**) R–Control, (**b**) GMA, (**c**) SDS, (**d**) GMA–SDS, (**e**) GMA–GF, (**f**) SDS–GF.

The HDPE particle sizes in the GMA blend are smaller than the R–Control but also varying and tend to take the shape of elongated rods rather than spherical particles. The poor dispersion of HDPE in the GMA blend where the PET is the major phase could be due to the low viscosity of PET, as in another study [48] the dispersion of HDPE was better when the blend was PE-rich. Even though the interfacial tension plays an important role in determining the final droplet size, the viscosity ratio of the blend components is also

a key factor. The greater the viscosity of the blend, the lower the final droplet size of the dispersed phase [49].

The bright specks present in all the images except the R–Control blend belong to the antioxiant particles as they were added to the blends in the form of powder. The dispersion size of HDPE in the GMA blend was reduced to 55 μm, which means that the diameter was reduced to half its original size in the R–Control blend, taking into account that the largest length was measured in the GMA blend. Since the shape of the HDPE particles in the blends is not always spherical, an area analysis would provide a more accurate evaluation of size reduction in the morphology. The SDS blend shows smaller diameters of the HDPE phase and less droplet size variation than the GMA blend, proving a more homogeneous structure with particle size of 14 μm which is 87% smaller than the R–Control dispersions. In addition, the smaller droplet size means the surface area between the PET and HDPE is larger, due to the surface modification of PET from the SDS [37], which allowed the HDPE droplets to disperse better throughout the PET matrix. As for the GMA–SDS blend, the dispersion size reached 43 μm (61% decrease) with a wider size distribution throughout the blend. This wide variation could be attributed to the coalesence seen between two HDPE particles as seen in Figure 5d. This is observed in the remainder of the blend as well, where in some regions dispersion size is small meaning reduced interfacial tension and good adhesion, while in other regions the dispersion size is large, resulting in poor adhesion between HDPE and PET and thus less compatibility between the two phases [49].

This morphology hence supports why the combination of HDPE-g-MA compatibilizer with PET functionalization renders a blend with inadequate properties. The mix between these two has not been studied in the literature before, so it is hypothesized that when the PET was treated with SDS, the SDS micelles formed a shell around the PET chains [37], thereby blocking the interaction that occurs between the MA groups on the HDPE-g-MA compatibilizer and the hydroxyl groups of PET. Nonetheless, the SDS treatment was still able to lead to smaller HDPE dispersion sizes by lowering the interfacial tension between the two polymers. The GMA–GF blend and SDS–GF blend both show small sized droplets with diameters of 10 and 19 μm, respectively. This is due to the presence of the glass fibers, as it was reported in the literature that dispersion size is smaller in reinforced blends compared with the unreinforced counterparts [50].

Coating of the matrix onto the fibers is also seen which indicates good adhesion and ability of load transfer from the matrix to the fibers, improving the stiffness of the blend. However, in the SDS–GF blend, fiber pull-outs are spotted, which will lead to poor tensile properties of the blend. The reason behind the HDPE-g-MA providing a better adhesion to the matrix is the MA functionality which acts as a coupling agent between the blend matrix and the glass fibers [51].

3.1.3. Mechanical Properties

Tensile Test

The E-modulus of all blends is presented in Figure 6a. The R–Control blend showed a reasonably high E-modulus with a value of 1045 MPa, which means that the blend is stiff and brittle, due to the shorter polymer chains which result from chain scissions that have taken place during the lifetime of the polymers as well as during extrusion where the high temperature leads to thermal degradation and the shearing action of the screw induces mechanical degradation [51,52]. Furthermore, the inhomogeneous structure of the R–Control blend [53] in Figure 5a has large sized dispersions that act as crack initiators rendering a brittle blend. The E-modulus of GMA and GMA–SDS is lower than the R–Control blend by 23% and 18%, respectively. Such decrease is mainly due to the elastic nature of the HDPE-g-MA compatibilizer, meaning the blend is becoming more ductile [54]. This ductility is also supported by the SEM morphology, where the decrease in droplet size indicates better interfacial adhesion and compatibility between the two polymers [49].
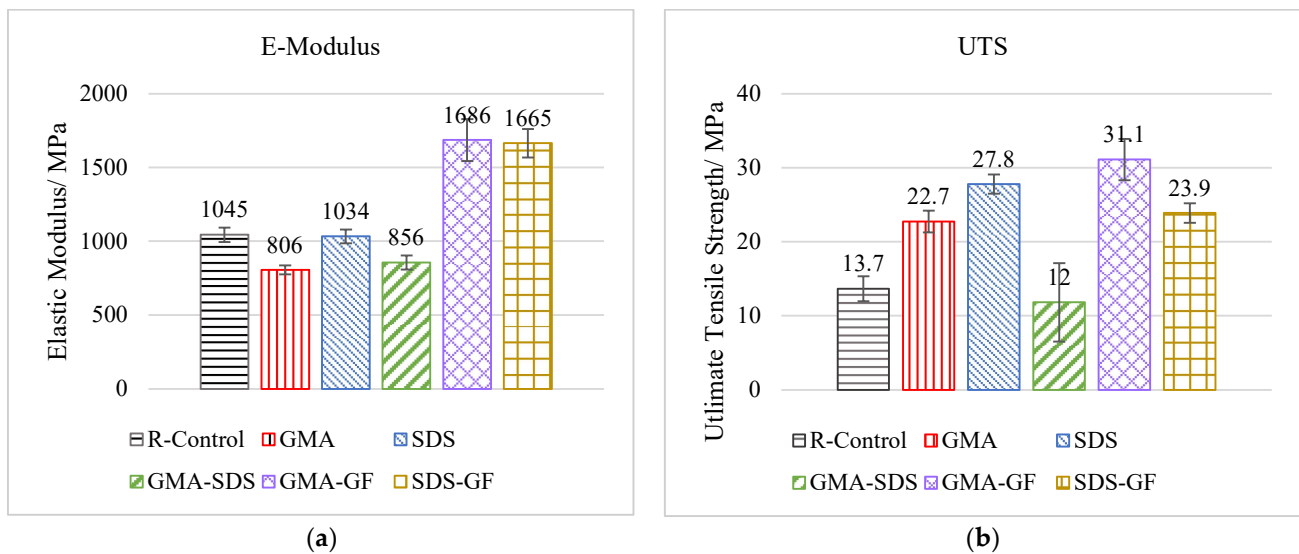
Figure 6. (**a**) Elastic modulus of blends (left), (**b**) ultimate tensile strength of blends (right).

The SDS blend shows almost no difference in stiffness in comparison to the R–Control. This is likely because the SDS functionalization works on lowering the HDPE size, enabling an even distribution of the minor phase but does not necessarily work on improving the adhesion between the two polymers. The blends with a higher E-modulus than the R–Control are GMA–GF and SDS–GF by 61% and 59%, respectively. This is due to the reinforcing action of glass fibers, which are known for increasing the stiffness of thermoplastics [49,54]. The GMA–GF and SDS–GF blends have stiffness values superior to those found in the literature for commonly used FDM materials such as ABS and PLA, which have E-modulus values ranging from 800 to 1600 MPa [55,56]. The UTS values of the blends are displayed in Figure 6b. The R–Control has a UTS of 13.7 MPa due to shorter chains of the recycled polymers withstanding lower values of stress. All the other blends have higher strength values than the R–Control, except for GMA–SDS. This can be referred to the morphology explained earlier in Section 3.1.1, where the blocking of the interaction between the compatibilizer and PET by the functionalization yielded a disturbance of the load transfer ability and hence lower mechanical properties. The highest average value is for the GMA–GF blend with 31.1 MPa, which is 127% better than the R–Control. This can be once more attributed to the reinforcing action of glass fibers [49,54], as well as the presence of the HDPE-g-MA which is a chemical coupling promoter between the polymer and GF surfaces [51].

The SDS functionalization facilitated the formation of crystallites giving a rise to the $\%X_c$, thereby increasing the UTS [37] wherein the UTS of the SDS blend showed a higher value than the R–Control by 103%. Taking into consideration that the lower dispersion size of the HDPE in the PET matrix is a sign of lower interfacial tension between the two phases, this led to the increase in strength, followed by SDS–GF and GMA which represented an increase of 74% and 66%, respectively. The weaker strength enhancing effect seen in the SDS–GF could be attributed to the weak fiber matrix adhesion which was observed in the SEM represented by the fiber pullouts. As for the GMA blend, the compatibilizer improved the ability of the blend to tolerate higher stress values due to better interfacial adhesion.

The blend with lower UTS and the highest standard deviation was for the GMA–SDS blend, possibly due to combining SDS with HDPE-g-MA compatibilizers, resulting in an inhomogeneous blend as mentioned before. The addition of GF to SDS led to a lower UTS by 14% compared to the SDS alone. Ronkay [50] reinforced PET-HDPE blends with GF and found that GF adhere better to the PET surface. So, this could signify that the PET surface functionalization yielded a PET surface which does not adhere well to the GF reinforcement, thereby lowering the maximum stress that can be tolerated by the blend. The UTS literature values of ABS and PLA range between 25 and 33 MPa [55–57] and the

blends that fit in this range are the GMA and GMA–GF blends. The evaluation of the %EL is illustrated in Figure 7a.
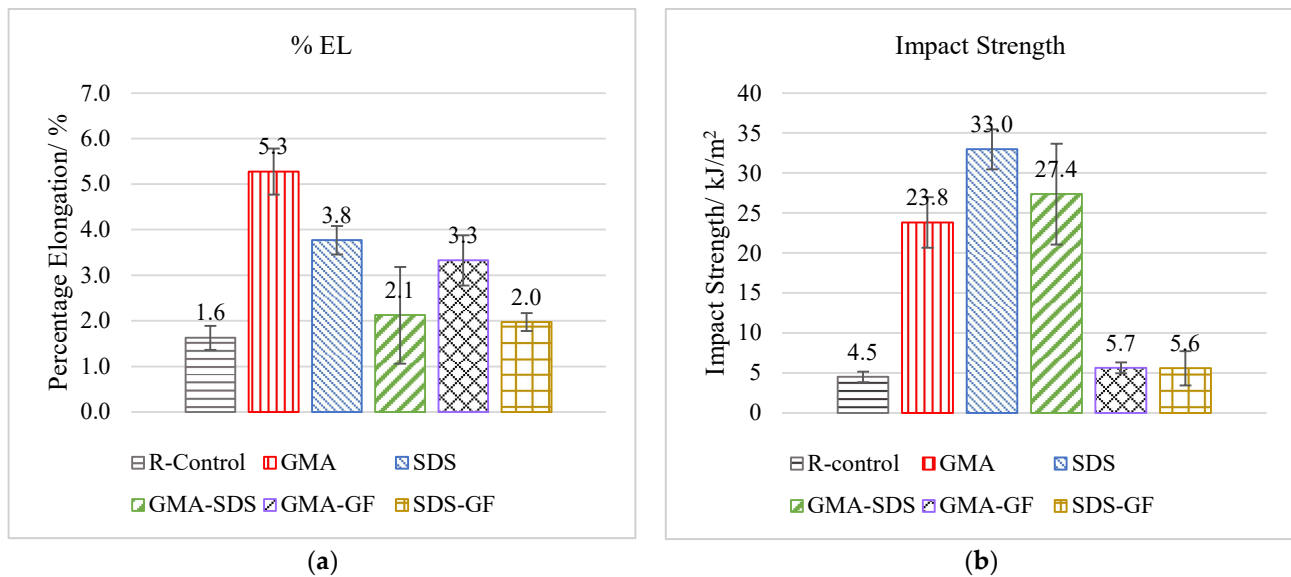
Figure 7. (**a**) Percentage Elongation of the blends (left), (**b**) impact strength of blends (right).

The lowest value of 1.6% is for the R–Control sample. In a study [58], it was mentioned that the compatibilization strength and how well the blend components adhere to each other are measured by the % EL. The most ductile sample was GMA with an elasticity of 5.3%, which is higher than the R–Control by 231%. This means that the HDPE-g-MA compatibilizer is able to locate at the interface between the two polymer phases and increase the interfacial adhesion, making the blend more ductile.

Following that come the SDS, GMA–GF, GMA–SDS, and finally the SDS–GF which are higher than the control by 138%, 106%, 31%, and 25%, respectively. The SDS functionalization provided lower ductility than the compatibilization method, indicating that the adhesion between the two polymer phases was not as efficient. It can also be seen that the GMA–SDS is lower than either GMA or SDS blend, which emphasizes the conclusion that SDS surface functionalization of PET might be blocking the interaction between the MA group of the HDPE-g-MA compatibilizer and the hydroxyl group of PET.

In addition, it should also be noted that the GMA–SDS blend has the highest standard deviation, possibly due to the wide diameter distribution of the minor phase in the blend. The least ductile blend after the R–Control is the SDS–GF with an % EL of 2%, which further proves how brittle the blend is, meaning SDS does not provide good adhesion between polymer blend matrix and reinforcement. In addition, since the GF increases the stiffness and UTS, then this denotes that the blend is becoming more rigid and less ductile, hence exhibiting a low value for % EL. The ductility of the GMA, SDS, and GMA–GF blends are comparable with that of commercial ABS (5–6%) and PLA (3–4%) [52,54].

Impact Test

The impact strength of all the blends is presented in Figure 7b. The impact strength of the R–Control blend is 4.5 kJ/m^2. This is due to the degradation in the recycled polymers which makes them stiff and brittle [58,59]. Furthermore, high interfacial tension between the two polymer phases facilitates fracture at the interface. The blends that provide the smallest rise in impact strength are the SDS–GF and GMA–GF, in which an increase of 24% and 27% is achieved, respectively. This agrees with the tensile results as the SDS–GF blend was the most brittle, further proving that the SDS does not offer the best properties when coupled with reinforcement. The HDPE-g-MA, however, gives a higher impact strength since the compatibilizer provides better adhesion between the fiber and matrix [60].

The glass fiber reinforced blends have a low impact strength, which is synonymous with the tensile test results, indicating that the short glass fibers are making the blend more brittle and less tough. Following this come the GMA, GMA–SDS, and SDS blend with 429%, 509%, and 633% increase in impact strength, respectively.

The SDS blend has a higher impact strength than the GMA blend, meaning that the blend absorbs more energy before fracture. This can be attributed to the smaller dispersion size of the HDPE nodules in the SDS blend in comparison to the GMA blend, meaning a greater interfacial area exists between the two polymers, giving the blend the ability to absorb more energy before fracture, thereby rendering a tougher blend. Despite the GMA–SDS having low tensile properties, it still had a high impact strength value, which could mean that the combination of the two methods serves better as an impact modifier. The highest standard deviation in the values was with the GMA–SDS blend, implying a lack of homogeneity in its structure as seen in the morphology.

3.1.4. Printability Assessment of Fractured 3D Printed Specimens

The preliminary printability assessment comprised of comparing between the computer-aided design (CAD) model and the printed specimens in terms of width, thickness, and cross-sectional area, and the quality of the tensile specimens were qualitatively evaluated from microscope images. Below, Figure 8 shows the microscope images of the top and cross-sectional view of the tensile samples after being laser-cut. Cross-sectional views are not necessarily an accurate way to evaluate the porosity content as the laser beam heats and melts the material during the cut, so diffusion of the material across layers will occur and might seal any porosities present. Starting with the R–Control sample in Figure 8a, several spacings between the longitudinal printed tracks can be observed. In the cross-sectional view, porosity can also be seen between the layers, this indicates a poor quality print of this blend. The GMA top view in Figure 8b clearly shows an irregular surface, and the printed tracks appear to contain some bubbles, possibly due to moisture that was trapped in the filament and released during printing [41] which may be due to inefficient drying of the filament [8]. The cross-sectional view shows no porosity in comparison with the R–Control. The SDS top view in Figure 8c shows a more uniform print with no inter-track spacing, indicating the good quality print provided by the functionalization method which provided lower dispersion size and greater surface area of contact between the two polymers. The cross-sectional view of the specimen shows no voids between the layers as well.

In Figure 8d, the GMA–SDS top view shows roughness and inconsistency along the length of the tracks and inter-track voids can also be seen. The cross-sectional view shows voids between the tracks in the layers approaching the end of the print. This could be due to the annealing effect from the heated build plate providing inter-diffusion between the bottom layers closest to the base, while the top layers were not subjected to this heat resulting in faster cooling and the presence of voids [41]. The GMA–GF top view presented in Figure 8e shows a rough surface appearance due to the presence of glass fibers, which increase the viscosity of the print, leading to lower flowability and greater interlayer spacing, as previously reported in the literature [61]. These inter-track voids can also be seen in the cross-sectional view of the sample. In addition, these samples were printed at 285 °C, which is 10 °C higher than the remaining blends, so this irregularity in the tracks can also be due to thermal degradation influencing the dimensional stability [12], or moisture that was trapped in the material and released, similar to the GMA blend. Finally, the SDS–GF top view in Figure 8f shows better surface appearance and consistency in the printed tracks than the GMA–GF sample but still exhibits some surface roughness. This could be due to the presence of fibers which disturb the flowability of the molten polymer matrix and lead to inter-track spacing as previously explained. The solution to this is either increasing the extrusion percentage from the nozzle beyond 100% [62] or decreasing the fiber content [63]. The brownish tint on the samples is due to the heating effect from the laser-cut. The irregular line in the middle of almost all the printed samples, except

the GMA–GF and SDS–GF, is due to the nozzle head passing by this region several times during the printing process, thereby causing friction and abrasion to the surface.

(a)

(b)

(c)

(d)

(e)

(f)
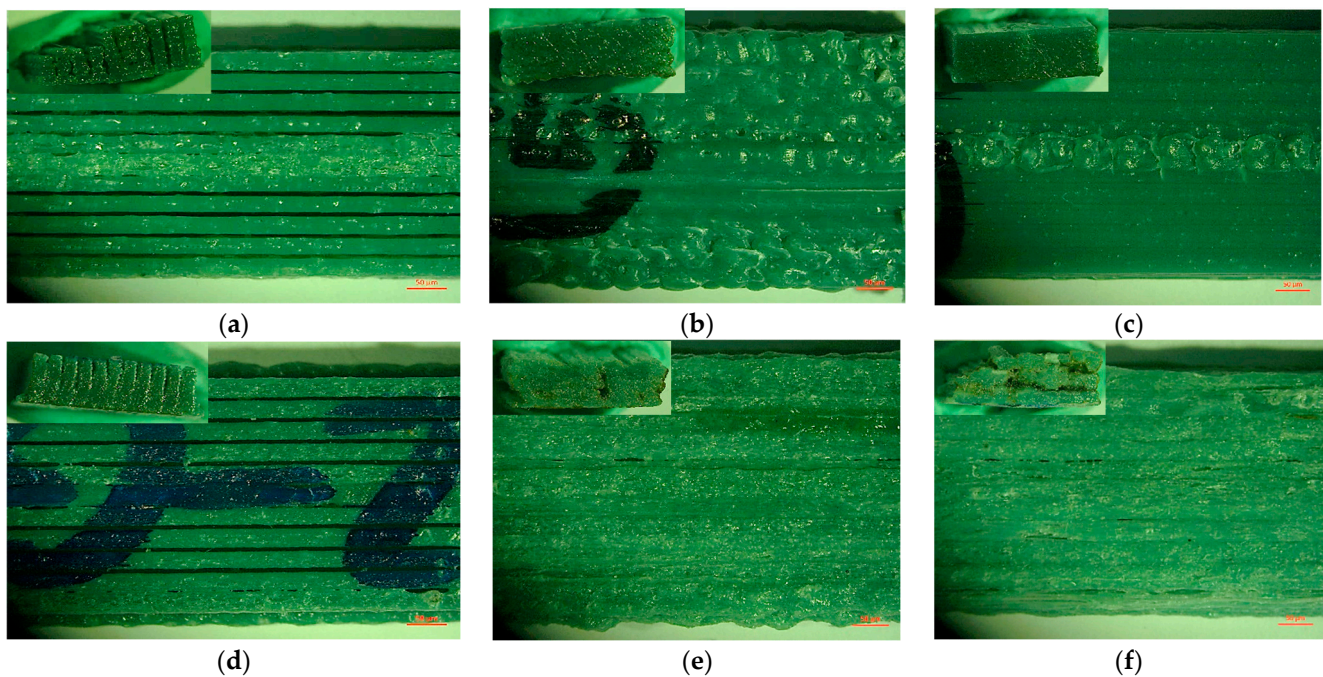
Figure 8. Top view of the surfaces of the 3D printed tensile samples: (**a**) R–Control, (**b**) GMA, (**c**) SDS, (**d**) GMA–SDS, (**e**) GMA–GF, and (**f**) SDS–GF. *Captures in the upper left corners are cross-sectional views after laser cut.*

The second part of the printability assessment is evaluating the dimensional accuracy of the printed products. The initial CAD dimensions of the cross-sectional area were 10.0 mm × 3.5 mm. The average width and thickness of the three printed specimens of each blend were measured using a micrometer and their standard deviation was calculated and is shown in Table 4. The area percentage increase was also calculated with respect to the CAD model. It should be noted that the GMA–GF samples printing was incomplete, so this led to a smaller cross-sectional area and, therefore, their area percentage increase was negative. From the overall average width and thickness, it can be seen that the sample width presents a large variation from the CAD model than the thickness, with an average increase in width of 0.73 mm (7.3%), while the average increase in thickness was 0.09 mm (2.5%). This is evident in Figure 9, which shows the datum line of the width and thickness of the CAD model along with the bar charts of the average dimensions of each blend.

Table 4. Average dimensions of 3D printed samples.

Blend Name	Width/mm	Thickness/mm
CAD Reference	10.00	3.5
R–Control	10.98 ± 0.31	3.78 ± 0.47
GMA	11.03 ± 0.65	3.69 ± 0.26
SDS	10.61 ± 0.46	3.77 ± 0.10
GMA–SDS	10.42 ± 0.23	3.64 ± 0.03
GMA–GF	10.59 ± 0.08	3.12 ± 0.81
SDS–GF	10.76 ± 0.17	3.56 ± 0.08

The bar charts of the width are much higher than their datum in comparison with the thickness and their corresponding datum. This difference can be linked to the path

width being larger than the nozzle diameter (0.96 vs. 0.8 mm), thereby depositing a greater amount of material from the nozzle during the print, which contributes to the low dimensional accuracy in the width of the samples. Since the filament is made in-house, filament diameter variations were definitely larger than those which are obtained industrially, and these deviations were not taken into consideration by the slicing software, which also could have led to these dimensional inaccuracies. Furthermore, part of this variation may be linked to the printer's process capability and the slicing software [64]. The largest standard deviation and percentage increase in area is in the R–Control, GMA, and GMA–GF blends. Some of the samples printed presented an irregular surface similar to that found in Figure 7b. This is assumed to be due to thermal degradation occurring during the printing process, or possibly due to moisture presence in the filaments being released with high temperature as stated earlier. The smallest standard deviation and percentage increase in area is in the GMA–SDS sample, which is likely due to a thin but consistent filament diameter which led to the inter-layer spacing seen in Figure 8d. Filament consistency and vacuum drying of the material and filaments would be needed in future work to be able to link the blend composition with dimensional accuracy.
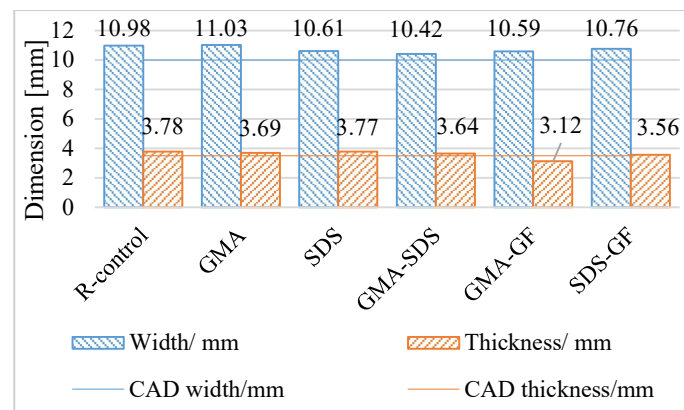
Figure 9. Dimensional comparison between the CAD model and printed parts.

3.1.5. Cost Estimation of Materials

The unit price of each of the components in the GMA and SDS blend were obtained, and their share in 1 kg of the blend was calculated to find the overall cost price of these blends. The GMA cost price of 1 kg is equivalent to USD 5 while the SDS blend is equivalent to USD 2. Their selling prices are set to be multiplied by 200% without shipment costs. So, the GMA blend selling price of a spool of 1 kg would be USD 10, while the SDS blend would be approximately USD 4. The selling prices obtained from online commercial websites had a selling price of VPETG spool equivalent to USD 25, while RPETG costs of around USD 20. The VHDPE spool cost is almost USD 60.

As can be seen, both blends would be more economical to use than the commercially available spools of similar material. Hence, it can be stated that the developed recycled blends will be less expensive than other virgin and recycled materials readily available in the market, and it will contribute to lower plastic waste generated by 3D printing, because users will be utilizing waste instead of generating new waste.

3.2. Life Cycle Assessment (LCA)

Figure 9 illustrates the model created for each blend, with all inputs into the system using Sankey diagram representation which visualizes the quantity of the flows in relation to the final product in terms of the arrows thickness. Figure 10 demonstrates the percentage contribution of each life cycle phase to the impact indicators and Table 5 demonstrates the cumulative impact of the life cycles assessed to each blend prepared for a set of impact categories.
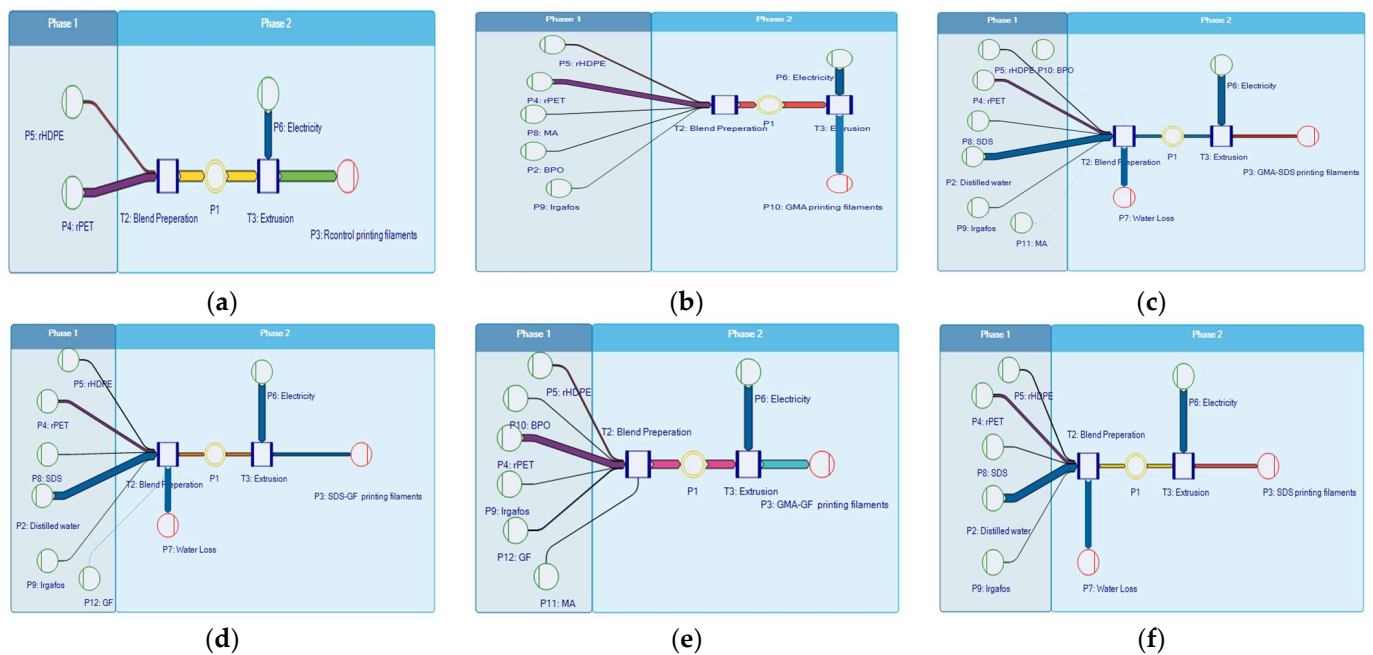
Figure 10. LCA Sankey diagram models for (**a**) R–Control, (**b**) GMA, (**c**) GMA–SDS, (**d**) SDS–GF, (**e**) GMA–GF, and (**f**) SDS.

Table 5. Life cycle impact assessment (LCIA) results in relation to functional unit of 1 kg for each blend.

	SDS–GF	SDS	R–Control	GMA–SDS	GMA–GF	GMA	V–Control
Freshwater ecotoxicity potential (FETP) no LT, kg 1,4-DCB-Eq	0.007630	0.007184	0.003163	0.004844	0.003669	0.003224	0.003655
Terrestrial acidification potential (TAP) no LT, kg SO_2-Eq	0.023808	0.022514	0.021770	0.022537	0.023481	0.022187	0.022900
Human toxicity potential (HTPc) no LT, kg 1,4-DCB-Eq	0.055101	0.050265	0.047578	0.049980	0.053134	0.048297	0.045087
Global warming potential (GWP1000) no LT, kg CO_2-Eq	12.678611	12.408651	12.271578	12.524416	12.723771	12.453811	12.795880
Particulate matter formation potential (PMFP) no LT, kg PM10-Eq	0.008117	0.007552	0.007264	0.007602	0.008017	0.007453	0.007774
Ozone depletion potential (ODPinfinite) no LT, kg CFC-11-Eq	0.000004	0.000035	0.000003	0.000003	0.000004	0.000003	0.000007
Water consumption potential (WCP) no LT, m3	0.035909	0.034358	0.022370	0.030769	0.027236	0.025684	0.030122
Fossil fuel potential (FFP) no LT, kg oil-Eq	4.476042	4.406701	4.372121	4.468671	4.521112	4.451771	4.794605

The set of selected impact categories is demonstrated in Table 5 for each blend prepared along with Figure 10 which demonstrates the quantitative data graphically. We show that for the freshwater eco-toxicity potential, terrestrial acidification potential, human toxicity potential, particulate matter formation, and water consumption potential the SDS–GF blend has the highest impact; followed by the V–Control blend with highest global warming potential and fossil fuel potential; and the SDS blend which has the highest ozone depletion potential.

The results in Figures 11 and 12 show the impact for each blend with a system boundary assigned cradle-to-gate, taking into consideration all the upstream activities for the raw material extraction and the manufacturing phase with all manufacturing energy consumption to achieve the FDM filaments. Calculations were carried out to provide the percentage contribution of each selected impact indicator to the life cycle phases being assessed and the results are summarized in Figure 11.
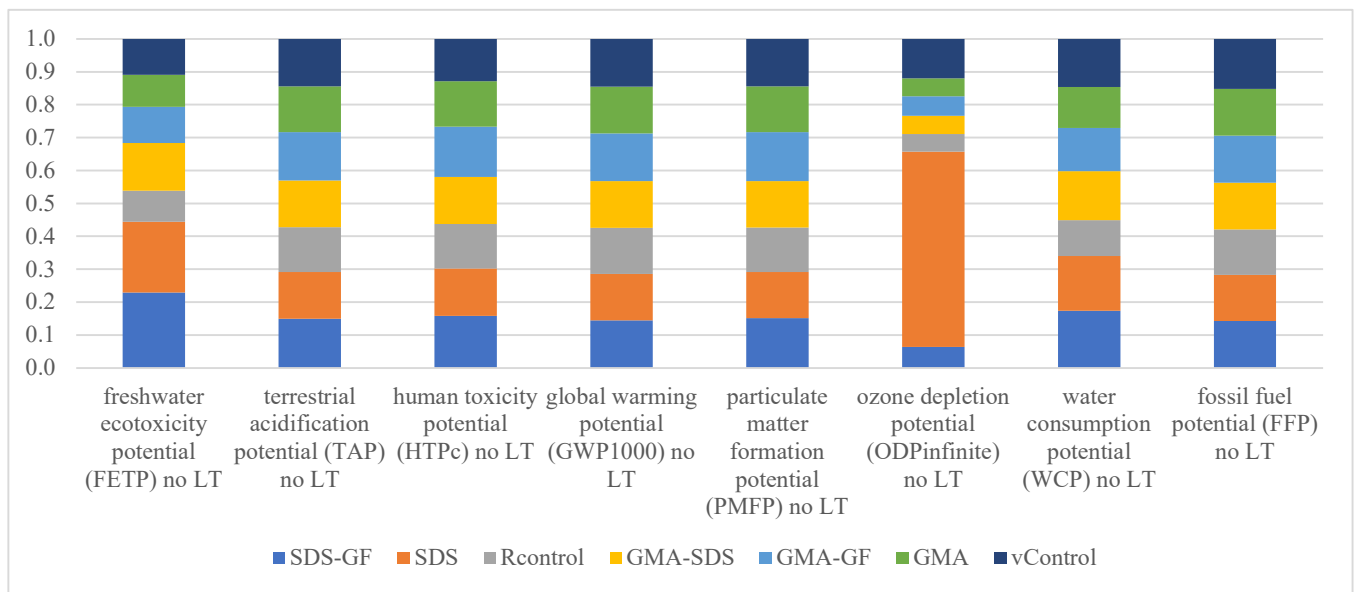
Figure 11. Representation of the life cycle impact (LCIA) results with 1 kg functional unit for each blend.
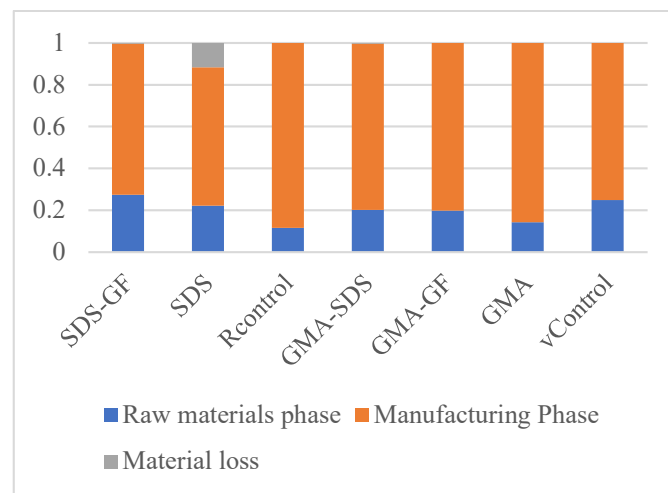

Figure 12. Percentage contribution of life cycle phases.

The raw materials phase takes into consideration the impacts from all upstream activities for the raw material extraction, and the manufacturing phase takes into consideration the energy used in the procedure carried out to obtain the FDM filaments. The material loss takes into consideration the water disposed of, which was used for all blend preparations using the SDS functionalization technique for the SDS, GMA–SDS, and SDS–GF blends.

Each blend displays how each phase of the life cycle contributes to the total impact; the manufacturing phase contributes the most to the impact indicators for all the blends as the energy consumption is invariable for all the blends' preparation. Therefore, taking a deeper look at the raw material phase for instance, the R–Control blend is composed of fewer materials and hence has a lower impact in the raw material phase. Also, for example, the SDS–GF blend has the highest contribution from the raw materials phase due to the presence of reinforcing glass fibers with a huge environmental impact.

Figure 13 illustrates the normalized impact indicators for each blend; this was calculated to show the lowest to highest in relation to the environmental performance. The R–control blend shows least environmental impact and the V–control blend shows highest environmental impact cumulatively.
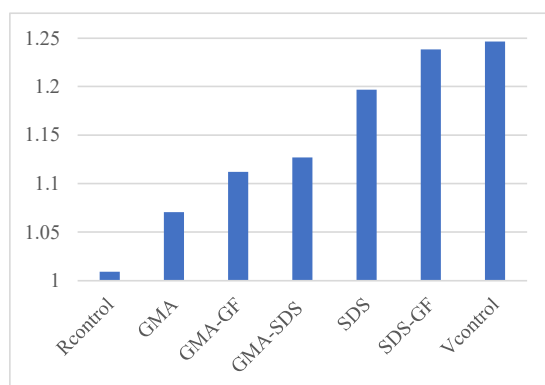
Figure 13. Normalized impact indicators.

4. Summary

This research aimed at the valorization of commodity plastic waste into feedstock material to be introduced for AM processes. Three main approaches were followed to develop the 80:20 rPET/rHDPE blends, namely: compatibilization, functionalization, hybridization, and reinforcement. The blends were assessed for their mechanical and thermal properties in addition to their printability.

The findings in this study are summarized in the Table 6.

Table 6. Collective summary of the properties and environmental impacts for all blends.

Blend Name	% Crystallinity HDPE/PET Phases	Glass Transition Temperature (°C)	E-Modulus (MPa)	Impact Strength (KJ/m²)	% Width Error in Prints	Cost Estimation (USD/Kg)	Fesh Water Eco Toxicity Potential (kg 1,4-DCB-Eq)	GWP (kg CO_2-Eq)
R–Control	64.8/18.0	97.27	1045	4.5	9.8	1.5	0.003163	12.27
GMA	24.7/22.9	95.26	806	23.8	10.3	5	0.003224	12.45
SDS	40.7/28.3	93.94	1034	33.0	6.1	2	0.007184	12.40
GMA–SDS	26.4/27.6	93.76	856	27.4	4.2	3.5	0.004844	12.52
GMA–GF	21.9/24.0	96.25	1686	5.7	5.9	6.5	0.003669	12.73
SDS–GF	35.9/22.9	96.78	1665	5.6	7.6	3.5	0.007630	12.67

5. Discussion

The growing plastic waste volume poses a threat to our eco-systems, and one of the ways to deal with this dilemma is to recycle more plastics and consequently achieve circularity. In this work, new blends are developed for FDM filaments using post-consumer recycled plastics (rPET-rHDPE) and a full material and sustainability assessment was carried out.

Three different methods of producing recycled rPET-rHDPE blends were investigated by grafting MA on rHDPE to form HDPE-g-MA, functionalization of PET with SDS, and finally by combining the two methods which is a novel approach. The selected blends were then compounded with 10 wt.% glass fibers. The results showed that the compatibilization and functionalization methods provided an enhancement in tensile and impact properties, which was also supported by the morphology images. The highest elastic modulus was achieved by the GMA–GF and the SDS–GF, which proved an improvement by 61% and 59%, respectively, in comparison to the control sample. On the other hand, the most ductile sample was the GMA with an elongation of 5.3%, which is a 231% improvement compared to the control sample. The most brittle sample was the SDS–GF, with an % EL of only 2%. The impact properties of the blends show that the highest impact strength was achieved by the SDS (429%) followed by the GMA–SDS (509%), and finally the GMA (429%) when compared to the control sample. The 3D printing of the blends proved to be successful but with limited dimensional accuracy, whereas the best printable blend was the GMA–SDS with an area % error of 8.4 in comparison to 18.6% for the control blend. Therefore, proper drying of the material, monitoring of filament consistency during

extrusion, and process optimization are key to be able to yield a better quality 3D-printed part. The cost calculations proved the economic efficiency of deploying the developed blends where a cost reduction of more than 50% was estimated.

LCA normalized impact indicators showed that the SDS–GF yielded the highest impact among all blends at 23.8% higher than the reference control sample (R–Control). Comparing the impact of the virgin materials with same composition (V–control), it proved to have the maximum environmental impact and was 24.6% higher than the R–Control. Here it is worth highlighting the huge environmental impact of the virgin PET/HDPE blend which is comparable to the blend containing glass fibers with its known negative environmental impact. By combining the results of the LCA and the material development and characterization, it is obvious that the novel blends GMA–GF and GMA–SDS were the best performing, chosen in relation to mechanical properties, printing quality, cost, and overall environmental performance.

6. Future Prospects

The authors believe that this research will bring the AM industry a step closer towards a circular economy by reducing the amount of virgin raw material resources, while reducing the amount of cumulative plastic waste generated by this industry. Furthermore, blends such as the GMA–GF present tensile properties similar to that provided by commonly used FDM commercial feedstock materials and thus can be used in AM applications such as prototype modeling. Simultaneously, the use of recycled feedstock material consumes and reduces the cumulative plastic waste volume already present whilst at the same time still being more economical than the standard raw material. In addition, future research is still required to study the effect of recycling cycles on the mechanical and thermal performance of the developed blends.

Author Contributions: Conceptualization: A.R. (Amna Ramzy); methodology: A.R. (Amna Ramzy), investigation: R.E., A.R. (Amira Ragab), and A.R. (Amna Ramzy); resources: A.R. (Amna Ramzy); data curation: R.E., A.R. (Amira Ragab), and A.R. (Amna Ramzy); writing—original draft preparation: R.E. and A.R. (Amira Ragab); writing—review and editing, R.E., A.R. (Amira Ragab), and A.R. (Amna Ramzy); visualization, R.E. and A.R. (Amira Ragab); supervision: A.R. (Amna Ramzy) and S.S.; project administration, A.R. (Amna Ramzy); funding acquisition: A.R. (Amna Ramzy). All authors have read and agreed to the published version of the manuscript.

Institutional Review Board Statement: Not Applicable.

Data Availability Statement: Data will be available upon request from corresponding author.

Conflicts of Interest: The authors declare no conflict of interest.

References

1. Kumar, R.; Sharma, H.; Saran, C.; Tripathy, T.S.; Sangwan, K.S.; Herrmann, C. A Comparative Study on the Life Cycle Assessment of a 3D Printed Product with PLA, ABS & PETG Materials. *Procedia CIRP* **2022**, *107*, 15–20. [CrossRef]
2. Kreiger, M.A.; Mulder, M.L.; Glover, A.G.; Pearce, J.M. Life cycle analysis of distributed recycling of post-consumer high density polyethylene for 3-D printing filament. *J. Clean. Prod.* **2014**, *70*, 90–96. [CrossRef]
3. Ding, G.K.C. Life cycle assessment (LCA) of sustainable building materials: An overview. In *Eco-Efficient Construction and Building Materials*; Elsevier: Amsterdam, The Netherlands, 2014; pp. 38–62.
4. Ragaert, K.; Delva, L.; Van Geem, K. Mechanical and chemical recycling of solid plastic waste. *Waste Manag.* **2017**, *69*, 24–58. [CrossRef] [PubMed]
5. Geyer, R.; Jambeck, J.R.; Law, K.L. Production, use, and fate of all plastics ever made. *Sci. Adv.* **2017**, *3*, e1700782. [CrossRef]
6. Sanchez, F.A.C.; Boudaoud, H.; Camargo, M.; Pearce, J.M. Plastic recycling in additive manufacturing: A systematic literature review and opportunities for the circular economy. *J. Clean. Prod.* **2020**, *264*, 121602. [CrossRef]

7. Rejeski, D.; Zhao, F.; Huang, Y. Research needs and recommendations on environmental implications of additive manufacturing. *Addit. Manuf.* **2018**, *19*, 21–28. [CrossRef]

8. Zander, N.E.; Gillan, M.; Lambeth, R.H. Recycled polyethylene terephthalate as a new FFF feedstock material. *Addit. Manuf.* **2018**, *21*, 174–182. [CrossRef]

9. Herianto; Atsani, S.I.; Mastrisiswadi, H. Recycled Polypropylene Filament for 3D Printer: Extrusion Process Parameter Optimization. *IOP Conf. Ser. Mater. Sci. Eng.* **2020**, *722*, 012022. [CrossRef]

10. Chong, S.; Pan, G.-T.; Khalid, M.; Yang, T.C.-K.; Hung, S.-T.; Huang, C.-M. Physical Characterization and Pre-assessment of Recycled High-Density Polyethylene as 3D Printing Material. *J. Polym. Environ.* **2016**, *25*, 136–145. [CrossRef]

11. Tsai, H.-H.; Wu, S.-J.; Wu, Y.-D.; Hong, W.-Z. Feasibility Study on the Fused Filaments of Injection-Molding-Grade Poly(Ethylene Terephthalate) for 3D Printing. *Polymers* **2022**, *14*, 2276. [CrossRef]

12. Bakır, A.A.; Atik, R.; Özerinç, S. Effect of fused deposition modeling process parameters on the mechanical properties of recycled polyethylene terephthalate parts. *J. Appl. Polym. Sci.* **2020**, *138*, 49709. [CrossRef]

13. Hamod, H. Suitability of recycled HDPE for 3D printing filament. Degree Thesis, Arcada University of Applied Science, Helsinki, Finland, 2014; p. 52.

14. Vidakis, N.; Petousis, M.; Maniadi, A. Sustainable Additive Manufacturing: Mechanical Response of High-Density Polyethylene over Multiple Recycling Processes. *Recycling* **2021**, *6*, 4. [CrossRef]

15. Zander, N.E.; Gillan, M.; Burckhard, Z.; Gardea, F. Recycled polypropylene blends as novel 3D printing materials. *Addit. Manuf.* **2018**, *25*, 122–130. [CrossRef]

16. Chow, H.M.; Koay, S.C.; Choo, H.L.; Chan, M.Y.; Ong, T.K. Investigating effect of compatibilizer on polymer blend filament from post-used styrofoam and polyethylene for fused deposition modelling. *J. Phys. Conf. Ser.* **2022**, *2222*, 012006. [CrossRef]

17. Vaucher, J.; Demongeot, A.; Michaud, V.; Leterrier, Y. Recycling of Bottle Grade PET: Influence of HDPE Contamination on the Microstructure and Mechanical Performance of 3D Printed Parts. *Polymers* **2022**, *14*, 5507. [CrossRef]

18. Utracki, L.A.; Wilkie, C.A. *Polymer Blends Handbook*, 2nd ed.; Springer: New York, NY, USA, 2014.

19. Pietrasanta, Y.; Robin, J.-J.J.; Torres, N.; Boutevin, B. Reactive compatibilization of HDPE/PET blends by glycidyl methacrylate functionalized polyolefins. *Macromol. Chem. Phys.* **1999**, *200*, 142–149. [CrossRef]

20. Šenitková, I.; Bednárová, P. Life cycle assessment. *JP J. Heat Mass Transf.* **2015**, *11*, 29–42. [CrossRef]

21. Filimonau, V. Life cycle assessment. *Routledge Handb. Tour. Sustain.* **2015**, *6*, 209–220.

22. Utela, B.; Storti, D.; Anderson, R.; Ganter, M. A review of process development steps for new material systems in three dimensional printing (3DP). *J. Manuf. Process.* **2008**, *10*, 96–104. [CrossRef]

23. Iniguez, C.G.; Michel, E.; Gonzalez-Romero, V.M.; Gonzalez-Nunez, R. Morphological stability of postconsumer PET/HDPE blends. *Polym. Bull.* **2000**, *45*, 295–302. [CrossRef]

24. Lei, Y.; Wu, Q.; Clemons, C.M.; Guo, W. Phase structure and properties of poly(ethylene terephthalate)/high-density polyethylene based on recycled materials. *J. Appl. Polym. Sci.* **2009**, *113*, 1710–1719. [CrossRef]

25. Taghavi, S.K.; Shahrajabian, H.; Hosseini, H.M. Detailed comparison of compatibilizers MAPE and SEBS-g-MA on the mechanical/thermal properties, and morphology in ternary blend of recycled PET/HDPE/MAPE and recycled PET/HDPE/SEBS-g-MA. *J. Elastomers Plast.* **2018**, *50*, 13–35. [CrossRef]

26. Tariq, A.; Ahmad, N.M.; Abbas, M.A.; Shakir, M.F.; Khaliq, Z.; Rafiq, S.; Ali, Z.; Elaissari, A. Reactive Extrusion of Maleic-Anhydride-Grafted Polypropylene by Torque Rheometer and Its Application as Compatibilizer. *Polymers* **2021**, *13*, 495. [CrossRef]

27. Ehrenstein, G.W.; Riedel, G.; Trawiel, P. *Thermal Analysis of Plastics*; Carl Hanser Verlag GmbH & Co. KG: Munich, Germany, 2004.

28. Pan, Y.; Wu, G.; Ma, H.; Zhou, S.; Zhang, H. Improved compatibility of PET/HDPE blend by using GMA grafted thermoplastic elastomer. *Polym. Technol. Mater.* **2020**, *59*, 1887–1898. [CrossRef]

29. ISO 180. Available online: https://yiqi-oss.oss-cn-hangzhou.aliyuncs.com/aliyun/technology/94265/14981.pdf (accessed on 25 June 2023).

30. ISO 14040. Available online: https://www.ag5.com/certifications/iso-14040/ (accessed on 25 June 2023).

31. ISO 14044. Available online: https://www.iso.org/standard/38498.html (accessed on 25 June 2023).

32. Ramzy, A.; Elfeky, A.; Aboulseoud, H.; Shihata, L.; Wohlgemuth, V. Resource and Energy Efficiency Analysis in Bottle-To-Bottle Recycling Plant—Case Study. In *Advances and New Trends in Environmental Informatics. ENVIROINFO 2021*; Springer: Cham, Switzerland, 2021; pp. 105–115. [CrossRef]

33. Ragab, A.; Ramzy, A. *Cradle-to-Gate Life Cycle Assessment of Bottle-to-Bottle Recycling Plant: Case Study*; Springer International Publishing: Berlin/Heidelberg, Germany, 2023.

34. Ragab, A.; Osama, A.; Ramzy, A. Simulation of the Environmental Impact of Industries in Smart Cities. *Ain Shams Eng. J.* **2023**, *14*, 2103. [CrossRef]

35. Torres, N.; Robin, J.J.; Boutevin, B. Study of compatibilization of HDPE-PET blends by adding grafted or statistical copolymers. *J. Appl. Polym. Sci.* **2001**, *81*, 2377–2386. [CrossRef]

36. Van Kets, K.; Delva, L.; Ragaert, K. Structural stabilizing effect of SEBSgMAH on a PP-PET blend for multiple mechanical recycling. *Polym. Degrad. Stab.* **2019**, *166*, 60–72. [CrossRef]

37. Cazan, C.; Cosnita, M.; Duta, A. Effect of PET functionalization in composites of rubber–PET–HDPE type. *Arab. J. Chem.* **2017**, *10*, 300–312. [CrossRef]

38. Pracella, M.; Rolla, L.; Chionna, D.; Galeski, A. Compatibilization and properties of poly(ethylene terephthalate)/polyethylene blends based on recycled materials. *Macromol. Chem. Phys.* **2002**, *203*, 1473–1485. [CrossRef]

39. Pluta, M.; Bartczak, Z.; Pawlak, A.; Galeski, A.; Pracella, M. Phase structure and viscoelastic properties of compatibilized blends of PET and HDPE recyclates. *J. Appl. Polym. Sci.* **2001**, *82*, 1423–1436. [CrossRef]

40. Tariq, A.; Afzal, A.; Rashid, I.A.; Shakir, M.F. Study of thermal, morphological, barrier and viscoelastic properties of PP grafted with maleic anhydride (PP-g-MAH) and PET blends. *J. Polym. Res.* **2020**, *27*, 1–10. [CrossRef]

41. Van de Voorde, B.; Katalagarianakis, A.; Huysman, S.; Toncheva, A.; Raquez, J.-M.; Duretek, I.; Holzer, C.; Cardon, L.; Bernaerts, K.V.; Van Hemelrijck, D.; et al. Effect of extrusion and fused filament fabrication processing parameters of recycled poly(ethylene terephthalate) on the crystallinity and mechanical properties. *Addit. Manuf.* **2021**, *50*, 102518. [CrossRef]

42. Jayanarayanan, K.; Thomas, S.; Joseph, K. Effect of compatibilizer on the morphology development, static and dynamic mechanical properties of polymer-polymer composites from LDPE and PET. *Int. J. Plast. Technol.* **2015**, *19*, 84–105. [CrossRef]

43. Jiang, C.-H.; Zhong, G.-J.; Li, Z.-M. Recyclability of In Situ Microfibrillar Poly(ethylene terephthalate)/High-Density Polyethylene Blends. *Macromol. Mater. Eng.* **2007**, *292*, 362–372. [CrossRef]

44. Zander, N.; Boelter, Z.R. Rubber toughened recycled polyethylene terephthalate for material extrusion additive manufacturing. *Polym. Int.* **2020**, *70*, 742–748. [CrossRef]

45. Menczel, J.D.; Prime, R.B. *Thermal Analysis of Polymers: Fundamentals and Applications*; John Wiley & Sons, Inc.: Hoboken, NJ, USA, 2008.

46. Carté, T.L.; Moet, A. Morphological origin of super toughness in poly(ethylene terephthalate)/polyethylene blends. *J. Appl. Polym. Sci.* **1993**, *48*, 611–624. [CrossRef]

47. Fasce, L.; Seltzer, R.; Frontini, P.; Pita, V.R.; Pacheco, E.; Dias, M. Mechanical and fracture characterization of 50:50 HDPE/PET blends presenting different phase morphologies. *Polym. Eng. Sci.* **2005**, *45*, 354–363. [CrossRef]

48. Jarukumjorn, K.; Chareunkvun, S. Compatibilization of Recycled High Density Polyethylene (Hdpe)/Polyethylene Terephtha-Late (Pet) Blends. *J. Sci. Technol.* **2006**, *14*, 1–8.

49. Yousfi, M.; Lepretre, S.; Soulestin, J.; Vergnes, B.; Lacrampe, M.-F.; Krawczak, P. Processing-induced degradation of nanoclay organic modifier in melt-mixed PET/PE blends during twin screw extrusion at industrial scale: Effect on morphology and mechanical behavior. *J. Appl. Polym. Sci.* **2013**, *131*. [CrossRef]

50. Shafiq, M.; Yasin, T.; Shaista, R.A.M. Structural, thermal, and antibacterial properties of chitosan/ZnO composites. *Polym. Polym. Compos.* **2013**, *16*, 101–113. [CrossRef]

51. Pritchard, G. *Plastics Additives an A-Z Reference*, 1st ed.; Springer: Dordrecht, The Netherlands, 1998.

52. Loultcheva, M.; Proietto, M.; Jilov, N.; La Mantia, F. Recycling of high density polyethylene containers. *Polym. Degrad. Stab.* **1997**, *57*, 77–81. [CrossRef]

53. Mancini, S.D.; Zanin, M. Recyclability of PET from virgin resin. *Mater. Res.* **1999**, *2*, 33–38. [CrossRef]

54. Lei, Y.; Wu, Q.; Zhang, Q. Morphology and properties of microfibrillar composites based on recycled poly (ethylene terephthalate) and high density polyethylene. *Compos. Part A Appl. Sci. Manuf.* **2009**, *40*, 904–912. [CrossRef]

55. Zweifel, H.; Maier, R.D.; Schiller, M. *Plastics Additives Handbook*, 6th ed.; Carl Hanser Verlag: Munich, Germany, 1991.

56. Cress, A.K.; Huynh, J.; Anderson, E.H.; O'neill, R.; Schneider, Y.; Keleş, Ö. Effect of recycling on the mechanical behavior and structure of additively manufactured acrylonitrile butadiene styrene (ABS). *J. Clean. Prod.* **2020**, *279*, 123689. [CrossRef]

57. Lay, M.; Thajudin, N.L.N.; Hamid, Z.A.A.; Rusli, A.; Abdullah, M.K.; Shuib, R.K. Comparison of physical and mechanical properties of PLA, ABS and nylon 6 fabricated using fused deposition modeling and injection molding. *Compos. Part B Eng.* **2019**, *176*, 107341. [CrossRef]

58. Kalfoglou, N.K.; Skafidas, D.S.; Kallitsis, J.K.; Lambert, J.-C.; Van der Stappen, L. Comparison of compatibilizer effectiveness for PET/HDPE blends. *Polymer* **1995**, *36*, 4453–4462. [CrossRef]

59. Pattanakul, C.; Selke, S.; Lai, C.; Miltz, J. Properties of recycled high density polyethylene from milk bottles. *J. Appl. Polym. Sci.* **1991**, *43*, 2147–2150. [CrossRef]

60. Torres, N.; Robin, J.; Boutevin, B. Study of thermal and mechanical properties of virgin and recycled poly(ethylene terephthalate) before and after injection molding. *Eur. Polym. J.* **2000**, *36*, 2075–2080. [CrossRef]

61. Polline, M.; Mutua, J.M.; Mbuya, T.O.; Ernest, K. Recipe Development and Mechanical Characterization of Carbon Fibre Reinforced Recycled Polypropylene 3D Printing Filament. *Open J. Compos. Mater.* **2021**, *11*, 47–61. [CrossRef]

62. Leong, J.J.A.; Koay, S.C.; Chan, M.Y.; Choo, H.L.; Tshai, K.Y.; Ong, T.K. Composite Filament Made from Post-used Styrofoam and Corn Husk Fiber for Fuse Deposition Modeling. *J. Nat. Fibers* **2021**, *19*, 7033–7048. [CrossRef]

63. Milosevic, M.; Stoof, D.; Pickering, K.L. Characterizing the Mechanical Properties of Fused Deposition Modelling Natural Fiber Recycled Polypropylene Composites. *J. Compos. Sci.* **2017**, *1*, 7. [CrossRef]

64. Chatham, C.A.; Zawaski, C.E.; Bobbitt, D.C.; Moore, R.B.; Long, T.E.; Williams, C.B. Semi-Crystalline Polymer Blends for Material Extrusion Additive Manufacturing Printability: A Case Study with Poly(ethylene terephthalate) and Polypropylene. *Macromol. Mater. Eng.* **2019**, *304*, 1800764. [CrossRef]